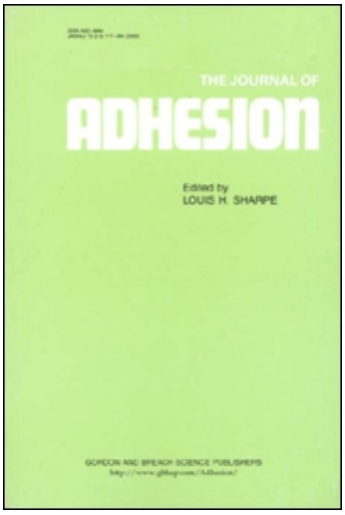

The Journal of Adhesion
Publication details, including instructions for authors and subscription information:
http://www.informaworld.com/smpp/title~content=t713453635

Analysis of the Symmetrical 90°-peel Test with Extensive Plastic Deformation

Q. D. Yang[a]; M. D. Thouless[b]; S. M. Ward[c]
[a] Dept. of Mechanical Engineering and Applied Mechanics, University of Michigan, Ann Arbor, MI, USA [b] Dept. of Materials Science and Engineering, University of Michigan, Ann Arbor, MI, USA [c] Scientific Research Laboratories, Ford Motor Company, Dearborn, MI, USA

To cite this Article Yang, Q. D. , Thouless, M. D. and Ward, S. M.(2000) 'Analysis of the Symmetrical 90°-peel Test with Extensive Plastic Deformation', The Journal of Adhesion, 72: 2, 115 — 132
To link to this Article: DOI: 10.1080/00218460008029274
URL: http://dx.doi.org/10.1080/00218460008029274

J. Adhesion, 2000, Vol. 72, pp. 115–132
Reprints available directly from the publisher
Photocopying permitted by license only

Analysis of the Symmetrical 90°-peel Test with Extensive Plastic Deformation

Q. D. YANG[a], M. D. THOULESS[a,b,*] and S. M. WARD[c]

[a] *Dept. of Mechanical Engineering and Applied Mechanics,*
[b] *Dept. of Materials Science and Engineering, University of Michigan, Ann Arbor, MI 48109, USA;* [c] *Scientific Research Laboratories, Ford Motor Company, Dearborn, MI 48121, USA*

(Received 6 April 1999; In final form 6 October 1999)

A numerical 2-D study of the symmetrical 90°-peel test (a similar geometry to the T-peel test) in which extensive plastic deformation occurs in the adherends is presented in this paper. A traction-separation relation is used to simulate failure of the interface, and the conditions for both crack initiation and steady-state crack growth are investigated. The numerical predictions for the steady-state peel force are compared with those based on elementary beam theory. It is shown that two competing effects dominate the mechanics of the peel test to such an extent that the results of beam-bending analyses cannot be used to predict the peel force. At one extreme range of parameters, delamination is driven by shear rather than by bending, resulting in a lower peel force than would be predicted by beam-bending analyses. At the other extreme, where delamination is bending-dominated, the constraint induced by the interfacial tractions cause an increase in the peel force. The numerical results are compared with the results of experiments in which adhesively-bonded specimens are tested in the symmetrical 90°-peel configuration. Excellent agreement between the numerical and experimental results validates the numerical approach.

Keywords: Adhesion and adhesives; fracture; fracture toughness; mechanical testing

1. INTRODUCTION

Adhesive bonding has received considerable interest in engineering applications such as automotive, aerospace and electronic packaging

*Corresponding author. Fax: 1-734-647-3170, e-mail: thouless@engin.umich.edu

industries. Compared with other joining techniques such as the use of nails, screws or rivets, adhesive bonding has many advantages. For example, it allows a more homogeneous stress distribution, improves the fatigue durability and provides weight savings [1].

The peel configuration is often used to study the failure of adhesively-bonded, thin, flexible laminates. Consequently, there have been many studies to analyze its behavior. Some of these analyses are subject to the limitation that the deformation of the adherends is dominated by elasticity during the fracture process [2–5]. It is well established that under these conditions, linear-elastic fracture mechanics (LEFM) provides a powerful tool for analyzing elastic peel joints. The force (per unit width) required to peel a flexible laminate from a semi-infinite substrate, P_f, is then a direct measure of the toughness of the joint, Γ, and is only dependent on the peel angle, φ [3]:

$$\frac{P_f}{\Gamma} = \frac{1}{1 - \cos\varphi} \tag{1}$$

For the symmetrical 90°-peel joints considered in this paper, this expression reduces to $P_f/\Gamma = 0.5$.

If the laminate is thinner than a critical value, given approximately by [6]

$$h_c \approx 6 E \Gamma / \sigma_y^2, \tag{2}$$

where E and σ_y are the elastic modulus and initial yield stress of the laminate, it will bend plastically before crack-growth begins. As a result, the use of LEFM is inappropriate because substantial amounts of energy may be dissipated by macroscopic plasticity in the laminate. Elasto-plastic fracture analyses are then necessary. Kim and Aravas [6] and Kinloch *et al.* [7] used beam theory to incorporate macroscopic plasticity into the analysis by using elasto-plastic relations between the bending moment and the radius of curvature for the laminate. However, these analyses neglected the cohesive stresses exerted at the crack-tip. Wei and Hutchinson [8] explored how the crack-tip plasticity induced by these stresses elevates the peel force above that predicted by using a value of the intrinsic toughness of the interface, Γ_0, in Eq. (1). This analysis of steady-state peeling was performed by coupling an embedded-process-zone model at the crack-tip [9, 10] to

an elementary-beam-theory model of the arm of the peel test. It was shown that if the maximum cohesive stress along the interface ($\hat{\sigma}$) is greater than about three times the yield stress of the laminate, the steady-state peel force (per unit width) increases dramatically with $\hat{\sigma}$. However, the results of Yang *et al.* [11] for the T-peel test suggest that a substantial elevation of the peel force can be obtained even when $\hat{\sigma}$ is relatively small, provided there is extensive plastic deformation in the arms of the laminate.

To investigate the comparison between analyses based on beam-bending and the cohesive-zone approach, the results of a comprehensive 2-D numerical analysis of the peel test are described in this paper. By directly incorporating the interaction of an appropriate traction–separation law for the interface with the plastic deformation of a laminate, the entire fracture process of a peel test from crack initiation to steady-state was simulated. The predictions of this full numerical model were validated by comparisons with experimental results using adhesively-bonded sheet metal. The relationship between the full numerical predictions presented here and analytical models based on elasto-plastic beam-bending theory are discussed in this paper, as well as a comparison with the results of Wei and Hutchinson [8].

2. RESULTS

2.1. Analytical Relationship Between Peel Force and Toughness

The derivation of an approximate relationship between the peel force and joint toughness provides a useful background to the results of the numerical modeling presented in the next section. The following derivation is based on an energy balance using elasto-plastic beam-bending theory, and essentially follows previous work of Kim and Aravas [6], Kinloch *et al.* [7] and Williams [12]. In the summary presented here, a symmetrical 90°-peel test is assumed, so that mixed-mode effects can be neglected. The laminates are assumed to exhibit rigid/plastic constitutive properties with isotropic power-law hardening, so that the stress, σ, and the strain, ε, are related by

$$\sigma = A\varepsilon^n; \tag{3}$$

where A and n are material constants. This is a suitable approximation provided the elastic strains are always negligible compared with the plastic strains; furthermore, it permits an analytical expression to be derived.

A schematic diagram of the symmetrical 90°-peel test is shown in Figure 1. The thickness of both laminates is h, and the interfacial toughness is taken to be Γ_0. At steady-state, a peeling force P_f (per unit width) is applied to each laminate in a direction perpendicular to the interface.[1] Dimensional analysis shows that

$$\frac{P_f}{\Gamma_0} = f\left[\frac{Ah}{\Gamma_0}, n\right]. \tag{4}$$

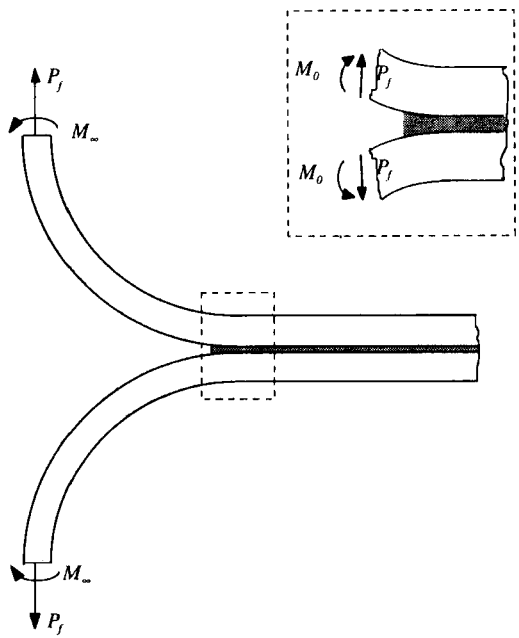

FIGURE 1 Beam-theory model of a symmetrical 90°-peel joint specimen. P_f and M_∞ are the applied peel force (per unit width) and remote bending moment (per unit width), respectively. At the crack-tip there is a resultant shear force, P_f, and bending moment, M_0, that act to open the crack.

[1]Since the laminates are clamped at 90° to the interface, there is also a remote bending moment of M_∞.

The remote loading has the effect of a bending moment, M_0, and a shear force, P_f, applied at the crack tip. If the crack advances by unit length, the peel force does work which is equal to P_f. This work must supply the energy for two processes – the energy of decohesion (Γ_0 per unit area), and the energy absorbed by plastic deformation in the laminates. Following previous analyses [6, 7, 12] it is assumed that bending dominates the decohesion process, and the effects of the shear force can be neglected. Consider an element of material which is initially undeformed far ahead of the crack tip. As the crack progresses, it enters the region in which the adhesive starts to deform, and the arms of the laminates are subjected to a bending moment that results from a combination of the applied loading and the forces imposed by the adhesive. These models assume that, at the crack tip, where the adhesive bonding has failed, the material element experiences an applied moment, M_0, which is dictated by the geometry and the applied load. The curvature of this point is $1/R_0$. Further crack propagation results in a decreasing bending moment being applied to the element, and eventually the element gets straightened out under reverse bending [6]. Assuming simple-beam theory applies, the moment-curvature relationship of this entire process can be calculated from Eq. (3), and is shown schematically in Figure 2. The area OABCO represents the energy absorbed by plastic bending (per unit width of laminate) as a crack advances by unit length. It can be calculated as

$$\frac{1}{\Gamma_0}\text{area[OABCO]} = \frac{1}{\Gamma_0}\oint_{\text{OABCO}} Md(1/R)$$
$$= \frac{2^{n+1}\sqrt{3}}{(n+1)}\left[\sqrt{3}(n+2)\right]^{1/n}\left(\frac{M_0}{Ah^2}\right)^{(n+1)/n}\left(\frac{Ah}{\Gamma_0}\right). \quad (5)$$

At steady-state, the difference between the work done by the external loads and the energy absorbed in bending must equal $\Gamma_0/2$ (the factor two enters because there are two arms that absorb energy, two applied loads doing work, but only one interface), *i.e.*,

$$\frac{P_f}{\Gamma_0} = \frac{\text{area[OABCO]}}{\Gamma_0} + \frac{1}{2}. \quad (6)$$

It has previously been shown [11] that, in the absence of cohesive stresses, the magnitude of the bending moment, M_0, that must be

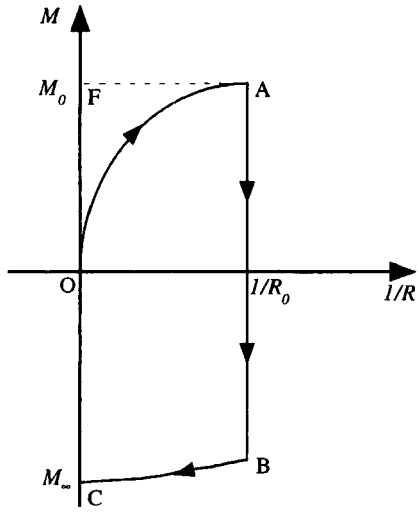

FIGURE 2 A typical bending history of a peeling laminate. M is the bending moment (per unit width), and R is the radius of curvature of the neutral axis of the deformed laminate. M_0 is the effective bending moment at the crack-tip, R_0 is the corresponding radius of curvature, and M_∞ is the remote bending moment exerted by the grips.

applied at the crack-tip to separate two arms having a constitutive law of the form given by Eq. (3) and bonded by an interface with a toughness of Γ_0 is given by

$$\frac{M_0}{Ah^2} = \left[\frac{2}{\sqrt{3}}\right]\left[\left(\frac{n+1}{4n}\right)^n \frac{1}{2(n+2)}\right]^{1/n+1}\left[\frac{\Gamma_0}{Ah}\right]^{n/n+1}. \tag{7}$$

Substitution of Eqs. (5) and (7) into Eq. (6) gives a result for the peel force based on the assumptions that bending dominates the decohesion process, and that the magnitude of any cohesive stresses are vanishingly small

$$\frac{P_f}{\Gamma_0} = \frac{1}{2} + \frac{2^n}{n}. \tag{8}$$

It should be noted that this remarkably simple analytical result arises because elastic deformations have been neglected. If elastic deformations are included in the analysis, Eq. (8) provides the asymptote for

the peel force when the laminate thickness, h, is much smaller than the critical thickness, h_c, defined in Eq. (2). In non-dimensional terms, this condition can be written as

$$\frac{Ah}{\Gamma_0} \ll 6\left(\frac{A}{\sigma_y}\right)\left(\frac{E}{\sigma_y}\right) \tag{9}$$

As the laminate thickness approaches h_c, the peel force must approach the asymptote of $P_f/\Gamma_0 = 0.5$, when there are no cohesive stresses. The analysis of Wei and Hutchinson [8] has shown that this small-scale yielding asymptote is substantially elevated if the cohesive peak stress, $\hat{\sigma}$, is greater than about $3\sigma_y$, where σ_y is the initial yield stress of the laminate.

2.2. Numerical Calculation of Peel Force

Numerical calculations were performed to investigate the relationship between the peel force, constitutive properties of the adherends, and the interfacial properties. These calculations incorporated an EPZ model of the type described in Yang *et al.* [11] into finite-element calculations using the ABAQUS (version 5.6) code [13]. Plane- and large-strain conditions were used, with the von Mises yield criterion and isotropic strain-hardening of the form given in Eq. (3) being assumed. In these calculations, the interface was replaced by user-defined elements that simulated an appropriate traction–separation relationship. This relationship, illustrated schematically in Figure 3, is characterized by Γ_0, the work of separation per unit area (equal to the area under the traction–separation curve), the peak stress supported by the interface, $\hat{\sigma}$, and two shape parameters δ_1/δ_c and δ_2/δ_c. Since an experimental study was an integral part of this project, the constitutive properties of the materials used in the experiments formed the basis for the parameters used in the numerical model.

In the formulation of the numerical calculations, the peak cohesive stress is an additional parameter not included in elementary energy-balance calculations of the type described in the previous section. It has been shown that this term has a profound influence on the results, whereas the shape parameters have a negligible effect in problems such

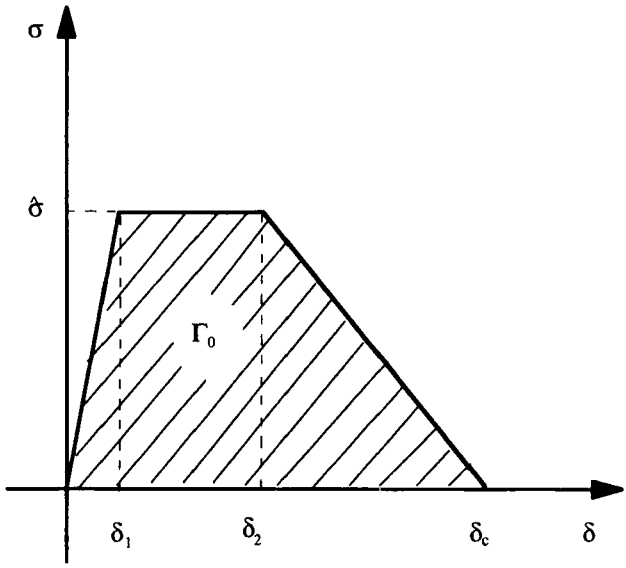

FIGURE 3 The traction–separation law used in the numerical analyses. It is characterized by a work of separation per unit area, Γ_0, a peak stress, $\hat{\sigma}$, and two shape parameters, δ_1/δ_c and δ_2/δ_c.

as this, where delamination is driven by a remote applied load [10]. Therefore, the dimensionless expression for the peel force must include an extra term, so that

$$\frac{P_f}{\Gamma_0} = f\left[\frac{Ah}{\Gamma_0}, \frac{\hat{\sigma}}{A}, n\right] \tag{10}$$

This equation is plotted in Figures 4 and 5 using the results obtained from the numerical calculations. Figure 4 shows how the numerically-predicted peel force varies with the parameter Ah/Γ_0. In distinct contrast to the results of the energy-balance calculations, the numerical results tend to an asymptotic limit of $P_f/\Gamma_0 = 0.5$ at very low values of Ah/Γ_0. At large values of this parameter, the peel force is somewhat higher than that predicted analytically; however, this discrepancy decreases with lower values of the parameter $\hat{\sigma}/A$. Figure 5 shows how the peel force varies with $\hat{\sigma}/A$, demonstrating the strong influence of the cohesive stress.

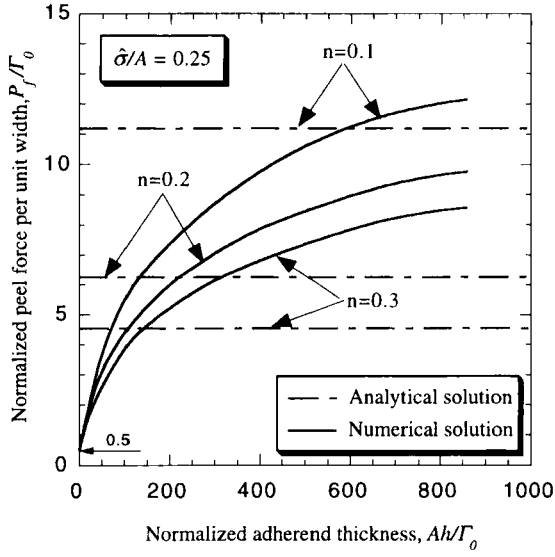

FIGURE 4 Normalized peel force (per unit width) plotted as a function of normalized laminate thickness.

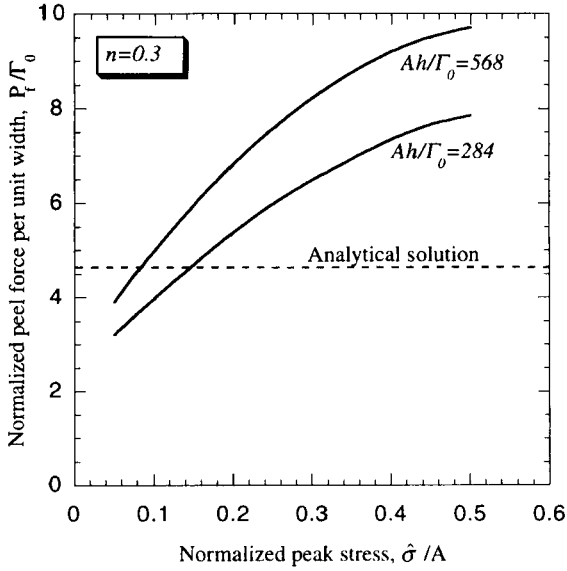

FIGURE 5 Normalized peel force (per unit width) plotted as a function of normalized peak stress.

2.3. Experimental Measurement of the Peel Force

Symmetrical 90°-peel test specimens were fabricated using coupons cut from aluminum (5754 Al, from Alcan Rolled Products Company) sheets of thickness $h = 1.0$ mm and $h = 2.0$ mm, and bonded by a commercial adhesive (Ciba Specialty Chemicals, XD4600). The thickness of the adhesive layers was maintained at a constant value of about 0.25 mm by using uniform-sized silica spheres as spacers. The width of the joint was 20 mm. Prior to bonding, each coupon was bent into the approximate shape shown in Figure 1, so as to enable steady-state to be reached more quickly during the peel test. The top parts of the specimens were held in the grips of a tensile testing machine, and peel-force *vs.* cross-head-displacement curves were recorded as the specimens were broken. A series of tests were performed for each thickness of aluminum. Each test was performed at room temperature, with a cross-head velocity of 50 mm/min.

Comparisons between the experimental and numerical results for the peel force (per unit width) *vs.* cross-head displacement are shown in Figure 6. In this figure, the shaded curves show the approximate range of the experimental results, and the points represent the results of numerical simulations using the following values for the material parameters: $\hat{\sigma} = 100$ MPa, $\Gamma_0 = 1.4\,\mathrm{kJm}^{-2}$, $A = 367$ MPa and $n = 0.238$. It should be emphasized here that the values of these parameters came from an independent study using a wedge geometry [11, 14]. There was no modification of the parameters before they were incorporated directly into the present simulations. The numerical results agree very well with the experimental data. They reproduce the steady-state values of the peel forces and do a fairly good job of mimicking the form of the experimental force-displacement curves.[2] Figure 7 summarizes the predicted effect of adherend thickness on the steady-state peel force (per unit width), and compares the predictions with the experimental results. This figure emphasizes the excellent agreement between the experimental results and the numerical predictions, which is particularly satisfying since all the parameters used in the simulation came from independent measurements.

[2]During the tests, samples tended to rotate slightly. This was responsible for much of the experimental scatter, and generated some variations in the precise form of the force-displacement curves.

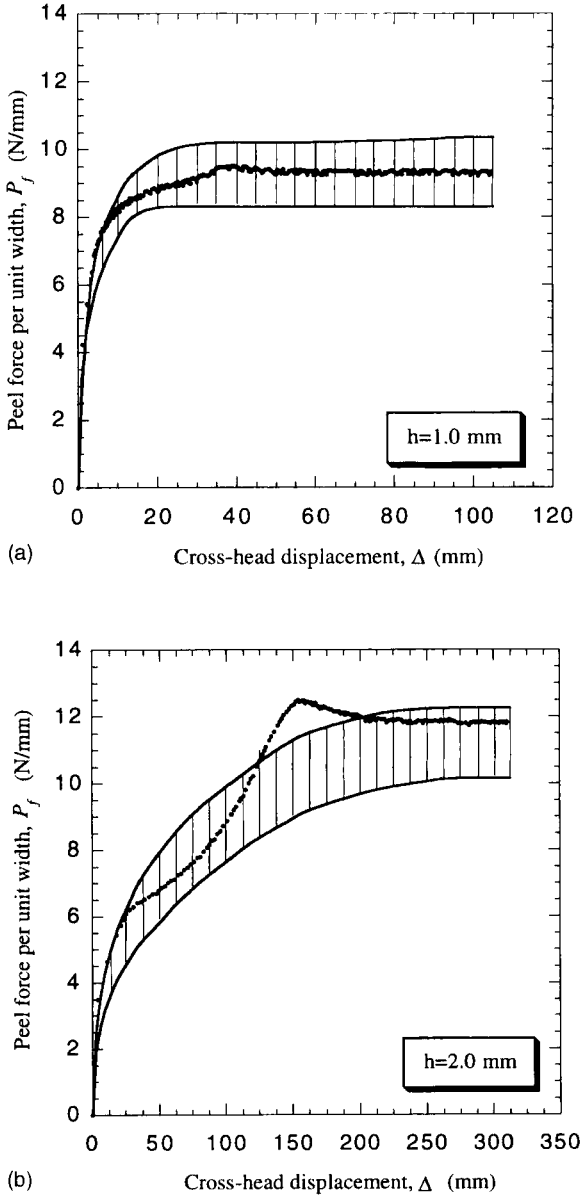

FIGURE 6 The peel force (per unit width) required to fracture the (a) 1.0 mm and (b) the 2.0 mm thick symmetrical 90°-peel specimens plotted as a function of cross-head displacement. The shaded curves show the approximate range of the experimental results. The points show the results of numerical simulations with $\Gamma_0 = 1.4\,\text{kJ/m}^2$ and $\hat{\sigma} = 100$ MPa.

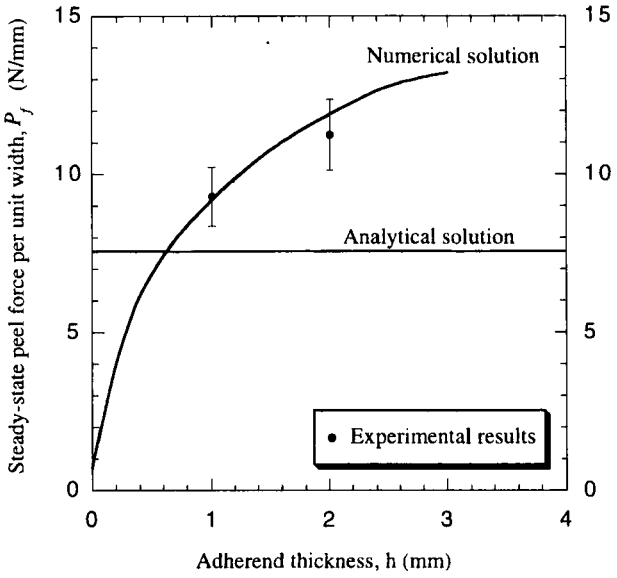

FIGURE 7 The peel force (per unit width) plotted as a function of laminate thickness. The solid line shows the result of numerical simulations with $\Gamma_0 = 1.4\,\text{kJ/m}^2$ and $\hat{\sigma} = 100\,\text{MPa}$.

3. DISCUSSION

Figures 6 and 7 show that the numerical results do an excellent job of predicting the behavior of the 90°-peel specimens. However, it can be seen that the results of the energy-balance calculations have little relationship to the observed behavior. In particular, the analytical results fail to capture the dependence of the peel force on the thickness of the adherends. The form of the analytical calculations suggests that the curvature and the critical crack-tip bending moment required for delamination are related in such a fashion that the total energy absorbed and the peel force should both be independent of the thickness of the laminate (where the thickness, h, is assumed to be much smaller than h_c, so plasticity dominates the bending deformation). This is contrary to both the numerical and experimental results. The discrepancy arises because, as the thickness of the adherends decreases, the magnitude of the bending moment decreases relative to the shear force acting at the crack tip. At lower values of Ah/Γ_0, when

both the radius at the crack-tip, R_0, and the effective bending moment, M_0, are very small, delamination is dominated by shear rather than the bending assumed in Section 2.1 and in previous analyses [6, 7, 12]. Under conditions where the energy dissipated by bending is negligibly small compared with the toughness, Γ_0, the peel force tends to the limit of $P_f/\Gamma_0 = 0.5$. The assumption that peeling is dominated by bending is valid only for large values of the dimensionless quantity Ah/Γ_0.

Although bending is expected to dominate the peeling process when Ah/Γ_0 is large, Figure 4 shows that in this range the analytical solution can substantially under-estimate the peel force. This is caused by the normal interfacial tractions, which are neglected in the analytical derivation. The normal stresses exerted on the adherend within the process zone (Fig. 8) induce an increased state of triaxiality which

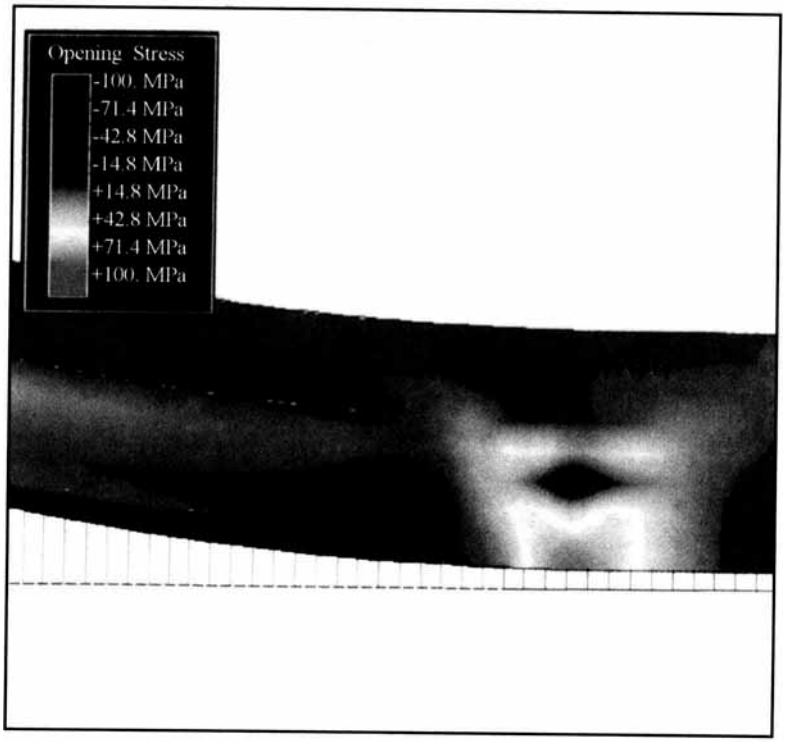

FIGURE 8 The distribution of the opening stresses near the crack tip (at steady-state) for a symmetrical 90°-peel joint (1.0 mm thick). (See Color Plate I).

makes it more difficult for yield to occur. Figure 9 shows the distribution of the von Mises stresses in the crack tip region during steady-state peeling; the bigger zone of yielding on the traction-free, compressive surface of the adherend can be clearly seen. More importantly, it is found that the stress distribution in this region is asymmetric about the neutral axis. Therefore, during steady-state, the peeling arm behind the current crack-tip experiences asymmetric strain-hardening and does not deform as elementary beam theory would predict. Figure 10 compares the bending history of an element of material in the 1.0 mm thick specimen as the element passes from a region far ahead of the crack tip to the remote arms of the peel specimen, during steady state, with what would be expected from the use of beam-theory. It can be seen that there is a substantial deviation between the two curves. The hysteresis curve predicted numerically is

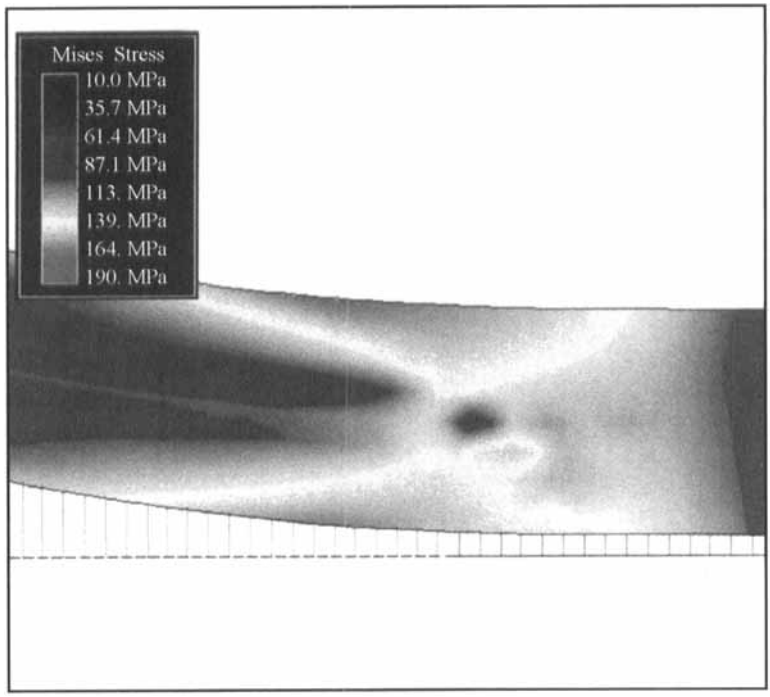

FIGURE 9 The distribution of the von Mises stresses near the crack tip (at steady-state) for a symmetrical 90°-peel joint (1.0 mm thick). (See Color Plate II).

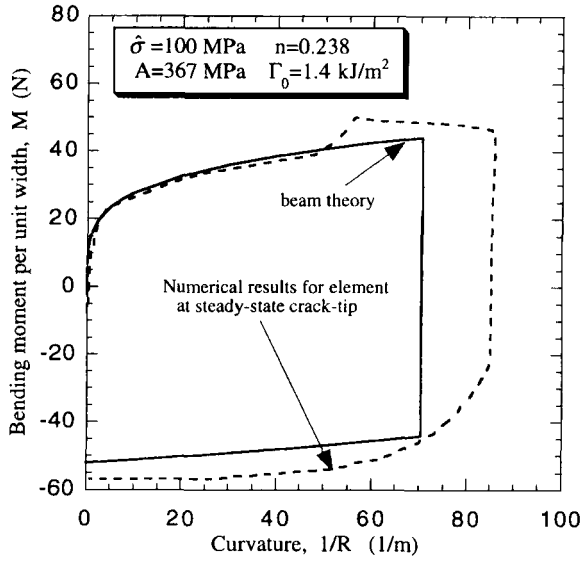

FIGURE 10 Comparison between the analytical and numerical results for the bending history of an element of material in the 1.0 mm thick, symmetrical 90°-peel specimen, as it passes from a region far ahead of the crack-tip to the remote arm during steady-state. The point at which the moment acting on the element shows a distinct jump in the numerical results corresponds to the location of the maximum opening stress at the interface.

significantly larger than the analytical curve. The increased energy dissipation that this implies is responsible for the larger peel force. It should also be noted that in beam-bending analyses it is implicitly assumed that the maximum bending moment corresponds to the maximum curvature of the laminate. However, it is very clear from Figure 10 that this assumption is not true if interfacial stresses are considered. Rather, the maximum bending moment occurs somewhere between the crack tip and the end of the process zone. Failure to account for this leads to significant errors in the peel-force predictions owing to the sensitivity of the peel force on the moment.

In summary, there are two competing effects that conspire to make the beam-bending approach of limited utility in predicting peel forces. When the value of Ah/Γ_0 is small, crack propagation is dominated by an opening rather than a bending mode, and the analytical result over-estimates the peel force. At large values of Ah/Γ_0, when bending dominates crack propagation, the effect of interfacial stresses is to

constrain the plastic bending of the adherends, so the analytical result is actually a lower-bound to the peel force. These two effects are directly analogous to the those described in previous work for wedge-induced delamination, Yang *et al.* [11]. There is a very strong dependence on the magnitude of the interfacial stress, even when it is relatively small (Fig. 5).

Wei and Hutchinson [8] have also shown how important the peak interfacial stress is for the fracture of a peel specimen. However, the origin of the elevated peel force that they describe is subtly different from that described in the present paper. In the work of Wei and Hutchinson [8], the crack-tip stresses *enhance* crack-tip plasticity. Provided the peak stress is greater than about three times the yield stress of the adherend, their results predict a dramatic increase in the peel force (above the value of the interfacial toughness) which is associated with increased energy dissipation in a process zone around the crack tip. The present study examines a different range of parameters for which there is a substantial amount of plasticity in the arms of the peel specimen. When bending dominates, the peel force is slightly greater than the magnitude of the interfacial toughness, owing to macroscopic plastic deformation in the arms. Furthermore, this peel force is increased by even small values of the cohesive strength because of a *diminution* of crack-tip plasticity owing to a triaxiality effect. It should be emphasized that the present results are valid for problems that are dominated by plasticity, and for which elastic strains can be neglected. A systematic study has shown that similar results are obtained when a full elastic–plastic constitutive law is used.

4. CONCLUSIONS

In this paper, the results of a rigorous 2-D numerical analysis of a symmetrical 90°-peel joint have been presented. The fracture process starting from crack initiation to steady-state crack growth has been simulated by replacing the interface with an appropriate traction–separation relation, which includes both the joint toughness and the maximum normal stress in the process zone. The numerical results demonstrate the importance of both interface parameters. In particular, approaches based on an energy-balance fail in two regards.

For small values of the adherend thickness, the assumption of bending-dominated crack propagation becomes invalid when the opening forces become significant. At the other extreme, the peak stress in the interface region affects the plastic deformation of the adherends. This has the effect of elevating the steady-state peel-force to levels considerably above those predicted by an energy-balance approach, so that, again, derivations based on simple beam-bending theory cannot be used reliably. Results from model experiments in which the interfacial bonding is provided by a commercial adhesive show excellent agreement with the numerical predictions using interface parameters obtained in a previous study [11].

A comparison of the results in this study with earlier analyses indicates that there are several regimes in the peel test that depend on a number of parameters. If the cohesive stresses are small (less than about three times the yield stress of the adherends), the peel force tends to a value of $\Gamma_0/2$ (for the symmetrical 90°-peel test) at both large and small values of the parameter Ah/Γ_0. At small values of this quantity, delamination is dominated by shear, rather than by bending, resulting in reduced plastic deformation. At large values of this quantity, the laminates deform elastically, and again, no plastic deformation occurs. At intermediate values, the laminates deform by plastic bending, and the peel force rises towards the asymptotic limit given by Eq. (8). Finite values of the cohesive stress result in a triaxial constraint, and the peel force is further elevated by this effect. The extent of the maximum in the peel force between the two limits is expected to depend also on the magnitude of σ_y/E; if this ratio is low, the transition from shear-dominated delamination to bending-dominated delamination will occur at the same time as the transition from plasticity-dominated bending to elasticity-dominated bending. When the cohesive stresses are relatively large (in excess of $3\sigma_y$), crack tip plasticity induced by the cohesive tractions becomes important. In this regime, the peel force will tend to the limit of $\Gamma_0/2$ for small values of Ah/Γ_0. However, at large values of Ah/Γ_0 the peel force will tend to a "small-scale yielding" limit that may be considerably elevated by the crack-tip plasticity [8]. Again, the extent of any peak in the peel force is expected to depend on the ratio of σ_y/E.

Different and sometimes competing effects have been described in the previous paragraph. These may result in various permutations of

beam-bending analyses giving approximate values for the peel force that sometimes appear to be consistent with experimental values. However, accurate interpretation of experimental data can only be achieved by the use of full numerical calculations of the type discussed in this paper.

Acknowledgments

This work was supported by Ford Motor Company and NSF Grant No. CMS9624452. The authors would also like to acknowledge invaluable discussions with J. W. Hutchinson during the course of this work.

References

[1] Kinloch, A. J., *Adhesion and Adhesives – Science and Technology* (Chapman and Hall Ltd., New York, 1987).
[2] Kaeble, D. H., *Trans. Society of Rheology* **4**, 45–52 (1960).
[3] Kendall, K., *Appl. Phys.* **8**, 1449–1452 (1973).
[4] Nicholson, D. W., *Internat. J. of Fracture* **13**, 279–293 (1977).
[5] Thouless, M. D. and Jensen, H. M., *J. Adhesion* **38**, 185–197 (1992).
[6] Kim, K. S. and Aravas, N., *Internat. J. Solids and Structures* **24**, 417–435 (1988).
[7] Kinloch, A. J., Lau, C. C. and Williams, J. G., *Internat. J. of Fracture* **66**, 45–70 (1994).
[8] Wei, Y. and Hutchinson, J. W., *Internat. J. of Fracture* **93**, 315–333 (1998).
[9] Needleman, A., *J. Appl. Mechanics* **54**, 525–531 (1987).
[10] Tvergaard, V. and Hutchinson, J. W., *J. Mech. and Phys. of Solids* **40**, 1377–1397 (1992).
[11] Yang, Q. D., Thouless, M. D. and Ward, S. M., *J. Mech. and Phys. of Solids* **47**, 1337–1353 (1999).
[12] Williams, J. G., *J. Adhesion* **41**, 225–239 (1993).
[13] *ABAQUS Finite Element Analysis Code and Theoretical Manual*, Version 5.6. (Hibbit, Karlsson and Sorensen, RI, 1996).
[14] Thouless, M. D., Adams, J. L., Kafkalidis, M. S., Ward, S. M., Dickie, R. A. and Westerbeek, G. L., *J. Mater. Sci.* **33**, 189–197 (1998).